

## A Heteronuclear Three-Dimensional NMR Experiment for Measurements of Small Heteronuclear Coupling Constants in Biological Macromolecules

GERHARD WIDER, DARIO NERI, GOTTFRIED OTTING, AND KURT WÜTHRICH

*Institut für Molekularbiologie und Biophysik, ETH-Hönggerberg, CH-8093 Zurich, Switzerland*

Received June 20, 1989

The use of high-resolution  $^1\text{H}$  NMR spectroscopy for the determination of the three-dimensional structure of proteins with molecular weights up to approximately 15,000 (1, 2) is by now well established. Present work on further improvements of the method is focussed on the one hand on the development of techniques that would enable studies of larger proteins. In this regard the use of 3D NMR (3), and especially the combination of isotope labeling, in particular with  $^{15}\text{N}$ , with heteronuclear 3D NMR experiments (4, 5) has already yielded promising results. On the other hand, much effort is also spent to further enhance the precision of protein structure determinations by NMR. In this context measurements of spin-spin coupling constants are a valuable complementation of the conformational constraints obtained from NOE experiments (2), both for the determination of direct constraints on individual dihedral angles (6, 7) and as input for establishing stereospecific assignments for prochiral groups of protons (8). For both purposes it has long been recognized that besides homonuclear  $^1\text{H}$ - $^1\text{H}$  couplings, heteronuclear coupling constants can provide important information (6, 9). This Communication describes a heteronuclear 3D NMR experiment which enables one to determine small heteronuclear couplings in crowded regions of protein NMR spectra, which would not be accessible for detailed analysis in the corresponding 1D or 2D NMR spectra.

Measurements of spin-spin coupling constants in the heteronuclear 3D NMR spectra rely on the fact that "incomplete" cross-peak fine structure patterns are obtained in homonuclear  $^1\text{H}$  2D NMR experiments when both correlated groups of protons have nonvanishing couplings with the same heterospin (10). This phenomenon arises because in the absence of a heteronuclear radiofrequency field the heterospins have the same spin orientation during the evolution time and the detection time. The separation of the two residual fine structure components along the two proton frequency axes is then equal to the respective heteronuclear coupling constants. This principle has been used by Wagner's group (11) for measurements of geminal and vicinal  $^{15}\text{N}$ - $^1\text{H}$  coupling constants in 2D  $^1\text{H}$  NMR experiments. The presently described 3D NMR experiment has the advantage of greatly improved spectral resolution, in particular in the crowded region of the  $\alpha$  and  $\beta$  protons, which is of special interest for conformational studies of proteins.

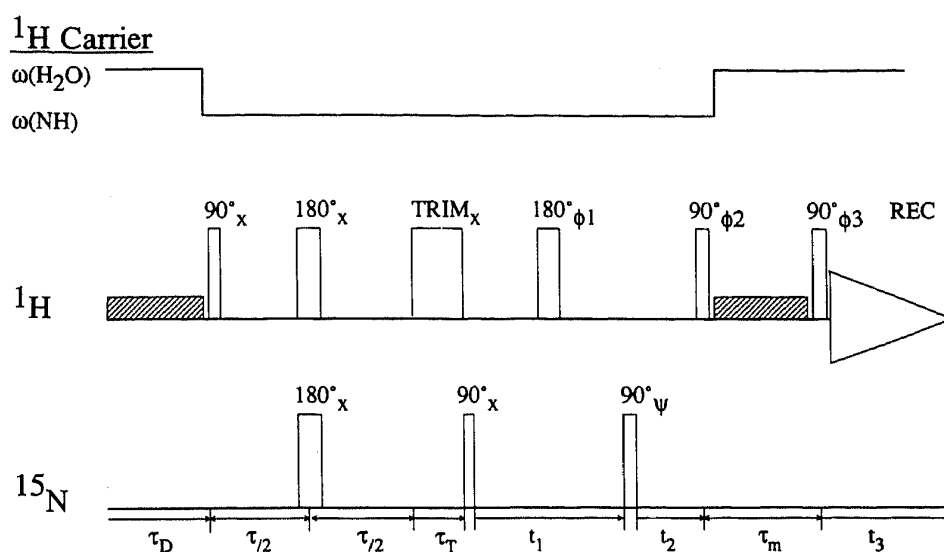


FIG. 1. Experimental scheme of the 3D [ $^{15}\text{N}$ ,  $^1\text{H}$ ]-correlated  $^1\text{H}$  NOESY experiment.  $\tau_D$  is the relaxation delay,  $\tau = 1/2J$  the evolution time of the heteronuclear coupling  $^1J(^{15}\text{N}, ^1\text{H})$ ,  $\tau_T$  the length of the trim pulse, and  $\tau_m$  the mixing time. The 3D data set was collected as a sequence of 2D experiments in  $t_1$  and  $t_3$  as a function of  $t_2$ . The  $\text{H}_2\text{O}$  resonance was suppressed by low power on-resonance continuous-wave irradiation during  $\tau_D$  and  $\tau_m$ . The pulse phases used are indicated in Table 1. The  $^1\text{H}$  carrier frequency was shifted between the  $\text{H}_2\text{O}$  position and the center of the amide proton chemical-shift range, as indicated at the top. Quadrature detection in the  $t_1$  dimension was achieved by applying, in addition to the phase cycling of Table 1, the TPPI method (13) to the first  $90^\circ$  ( $^{15}\text{N}$ ) pulse, and in the  $t_2$  dimension by using TPPI in concert for the first four proton pulses.

The experimental scheme of the presently used 3D NMR experiment (Fig. 1) first creates heteronuclear antiphase magnetization  $I_x S_z$  for the protons (spin I) that are directly bound to  $^{15}\text{N}$  (spin S). After the delay  $\tau$  the spin-lock pulse preserves

TABLE 1

Phase Cycling Used for Recording 3D [ $^{15}\text{N}$ ,  $^1\text{H}$ ]-Correlated  $^1\text{H}$  NOESY Experiments with the Scheme of Fig. 1

$\phi_1$	$\phi_2$	$\phi_3$	$\psi$	REC
x	x	x	x	x
x	x	x	-x	-x
-x	x	x	x	x
-x	x	x	-x	-x
x	-x	x	x	-x
x	-x	x	-x	x
-x	-x	x	x	-x
-x	-x	x	-x	x
x	x	-x	x	-x
x	x	-x	-x	x
-x	x	-x	x	-x
-x	x	-x	-x	x
x	-x	-x	x	x
x	-x	-x	-x	-x
-x	-x	-x	x	x
-x	-x	-x	-x	-x

the magnetization from  $^{15}\text{N}$ -bound protons, but randomizes by its RF inhomogeneity the magnetization from all other protons, which did not evolve during the delay  $\tau$  (12). The first  $90^\circ$  ( $^{15}\text{N}$ ) pulse transforms the antiphase magnetization  $I_x S_z$  into heteronuclear transverse two-spin coherence  $I_x S_y$ , which evolves during  $t_1$  and is converted back to proton magnetization  $I_x S_z$  by the second  $90^\circ$  ( $^{15}\text{N}$ ) pulse. Simultaneous phase alternation of the second  $90^\circ$  ( $^{15}\text{N}$ ) pulse and the receiver phase (Table 1) eliminates residual magnetization from protons not bound to  $^{15}\text{N}$  and selects for heteronuclear antiphase magnetization  $I_x S_z$ . The proton magnetization thus labeled with the  $^{15}\text{N}$  frequency is then subjected to a standard  $^1\text{H}$  NOESY experiment, with the evolution time  $t_2$ , the mixing time  $\tau_m$ , and the detection time  $t_3$ . During each scan the  $^1\text{H}$  carrier frequency is shifted between the water resonance position and the center of the amide proton chemical-shift range, as indicated by the top line in Fig. 1. This ensures on the one hand an optimal irradiation of the spectral range of interest in  $\omega_2$ , where only protons directly bound to  $^{15}\text{N}$  resonate, and on the other hand proper water irradiation and favorable conditions for detecting the full proton resonance range in  $\omega_3$ . In contrast to the previously proposed heteronuclear correlated  $^1\text{H}$  NOESY experiments (4, 5), the experiment of Fig. 1 does not include  $^{15}\text{N}$  decoupling, which reduces the effective sensitivity but ensures that the  $^{15}\text{N}$ - $^1\text{H}$  couplings are manifested along both  $\omega_2$  and  $\omega_3$ .

A 3D spectrum obtained with the experiment of Fig. 1 consists of a stack of parallel  $^1\text{H}$  NOESY planes, of which each contains cross peaks between a particular amide proton and all other protons. The NOESY planes are separated along the third frequency axis,  $\omega_1$ , by the different  $^{15}\text{N}$  chemical shifts of the individual nitrogen positions. Each individual  $^1\text{H}$  NOESY plane has an appearance similar to that of a 2D  $^1\text{H}$  NOESY spectrum of a  $^{15}\text{N}$ -labeled protein (11), except that they contain a much smaller number of cross peaks and the individual peaks are therefore better resolved. The cross peaks between the proton bound directly to  $^{15}\text{N}$  and additional  $^{15}\text{N}$ -coupled protons show the expected, incomplete E.COSY-type multiplet structure. From the peak separation along  $\omega_2$  the direct couplings  $^1J(^{15}\text{N}, ^1\text{H})$  can be determined, and the peak separation along  $\omega_3$  yields geminal and vicinal coupling constants with  $\text{H}^\alpha$  or  $\text{H}^\beta$ , as is indicated in Fig. 2.

As an illustration a [ $^{15}\text{N}$ ,  $^1\text{H}$ ]-correlated  $^1\text{H}$  NOESY experiment was recorded with the uniformly  $^{15}\text{N}$ -labeled N-terminal domain(1-69) of the 434 repressor (Fig. 2). This protein was produced from an overexpression system consisting of NM522 *Escherichia coli* cells (14), bearing a pRW190 plasmid obtained from Dr. G. Koudelka and Dr. M. Ptashne of Harvard University, Cambridge, Massachusetts. The cells were grown in a minimal medium containing  $(^{15}\text{NH}_4)_2\text{SO}_4$  (99.7%  $^{15}\text{N}$  enrichment, Isotec) as the sole nitrogen source, and the 434 repressor(1-69) was purified using a slight modification of the procedure of Anderson *et al.* (15), as described in detail elsewhere (16). For the NMR measurements we prepared a 12 mM solution of this uniformly  $^{15}\text{N}$ -labeled protein in  $\text{H}_2\text{O}$  at pH 5.0. The measurements were carried out on a Bruker AM 500 spectrometer equipped with a 5 mm inverse detection probe. The experimental parameters are given in the legend to Fig. 2. The resulting spectrum contained 64 homonuclear 2D  $^1\text{H}$  NOESY planes. Figure 2 presents contour plots of small spectral regions from three of these planes. Each of the four plots A-D displays a NOESY cross peak between an amide proton and an  $\alpha$  or  $\beta$

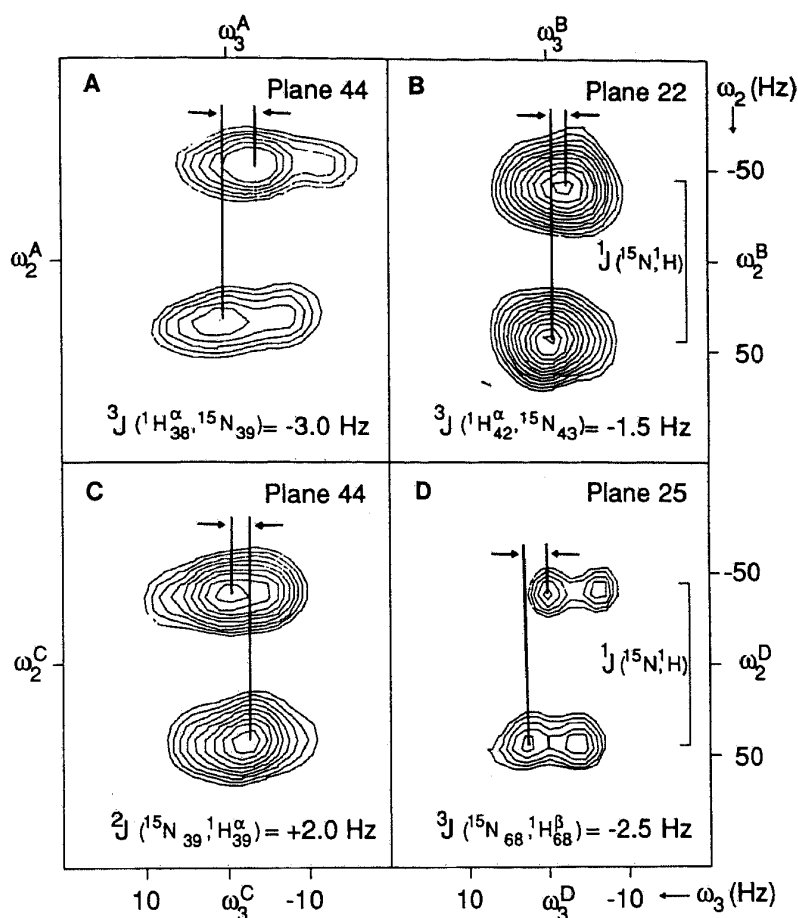


FIG. 2. Expanded contour plots from  $(\omega_2 - \omega_3)$  planes of a 3D [ $^{15}\text{N}$ ,  $^1\text{H}$ ]-correlated NOESY spectrum of a 12 mM  $\text{H}_2\text{O}$  solution of the uniformly  $^{15}\text{N}$ -labeled N-terminal domain (1–69) of the 434 repressor at 13°C and pH 5.0. The 3D time-domain data set consisted of 76, 108, and 2048 data points, respectively, in the  $t_1$ ,  $t_2$ , and  $t_3$  dimensions. Spectral widths of 1190, 2000, and 6024 Hz were chosen along  $\omega_1$ ,  $\omega_2$ , and  $\omega_3$ , which corresponds to values of  $t_{1\text{max}}$ ,  $t_{2\text{max}}$ , and  $t_{3\text{max}}$  of 32, 27, and 170 ms, respectively. The mixing time was 160 ms and the recycle delay was 1 s. For each free induction decay in  $t_3$ , 32 scans preceded by 4 dummy scans were accumulated, resulting in a measuring time of about four days. Before Fourier transformation, the time-domain data were multiplied with a cosine window in  $t_1$  and  $t_2$ , and with a sine bell shifted by  $\pi/10$  in  $t_3$ . After zero filling in all three dimensions the 3D Fourier transformation resulted in a real part of the 3D spectrum of 64, 256, and 4096 points in  $\omega_1$ ,  $\omega_2$ , and  $\omega_3$ . Only one-fourth of the data points along  $\omega_3$  could be retained at any one time because of data storage limitations. The following four cross peaks from three different NOESY planes are shown: (A) Sequential  $d_{\alpha\text{N}}$  connectivity between Lys 38 and Thr 39 at  $(\omega_2^{\text{A}} = 7.71 \text{ ppm}, \omega_3^{\text{A}} = 4.33 \text{ ppm})$ . (B) Sequential  $d_{\alpha\text{N}}$  connectivity between Pro 42 and Arg 43 at  $(\omega_2^{\text{B}} = 9.16 \text{ ppm}, \omega_3^{\text{B}} = 4.36 \text{ ppm})$ . (C) Intraresidual  $d_{\text{N}\alpha}(i, i)$  connectivity of Thr 39 at  $(\omega_2^{\text{C}} = 7.71 \text{ ppm}, \omega_3^{\text{C}} = 4.46 \text{ ppm})$ . (D) Intraresidual  $d_{\text{N}\beta}(i, i)$  connectivity at  $(\omega_2^{\text{D}} = 8.11 \text{ ppm}, \omega_3^{\text{D}} = 2.15 \text{ ppm})$ .

proton of the same or a sequentially neighboring residue. In all four examples the direct coupling constant  $^1J(^{15}\text{N}, ^1\text{H})$  observed along  $\omega_2$  is approximately 90 Hz.

Figure 2A shows the sequential connectivity  $d_{\alpha\text{N}}$  (2) between the residues Lys 38 and Thr 39. The displacement of the two components along  $\omega_3$  indicates that  $^3J(^1\text{H}_{38}^{\alpha}, ^{15}\text{N}_{39})$  is  $-3.0 \pm 0.7 \text{ Hz}$ . Use of this value with the Karplus-type calibration curve for this molecular fragment ( $\delta$ ) results in two possible values for the intervening

$\psi$  angle of about  $-15^\circ$  and  $-105^\circ$ , respectively;  $\psi = -105^\circ$  lies in a sterically unfavorable region of the Ramachandran diagram, which leaves  $\psi = -15^\circ$  as the only reasonable solution. This measurement is in good agreement with the X-ray structure of the N-terminal domain (1-69) of the 434 repressor (17). In this structure the residue Thr 39 is situated at the end of an  $\alpha$  helix, and  $\psi_{39}$  has a value of  $-26^\circ$ . Figure 2B displays the  $d_{\alpha N}$  cross peak between the residues Pro 42 and Lys 43, which are part of an extended region of the polypeptide chain. The  ${}^3J({}^1\text{H}_{42}^\alpha, {}^{15}\text{N}_{43})$  coupling constant of  $-1.5 \pm 0.7$  Hz corresponds to two sterically unfavorable values for the  $\psi$  angle of  $0^\circ$  and  $-120^\circ$ , and to two allowed values of  $95^\circ$  and  $145^\circ$ . The corresponding  $\psi_{42}$  value of  $162^\circ$  in the crystal structure is again quite close to one of the latter two possible solutions. For Thr 39 the intraresidual two-bond  ${}^{15}\text{N}-\alpha\text{H}$  coupling constant of  $+2.0 \pm 0.7$  Hz (Fig. 2C) lies well within the range of values reported earlier (6, 18). The different sign of this coupling constant relative to the vicinal couplings in Figs. 2A and 2B is readily detectable. In Fig. 2D the intraresidual NH- $\beta\text{H}$  cross peak of Val 68 is plotted. The displacement of the cross-peak components indicates a coupling constant of  $-2.5 \pm 0.7$  Hz. In the crystal structure, this  $\chi^1$  angle is not defined. Val 68 is the penultimate residue in the polypeptide chain and may thus have quite high rotational mobility about the  $\text{C}^\alpha-\text{C}^\beta$  bond. The rotational average for  ${}^3J({}^{15}\text{N}_i, \text{H}_i^\beta)$  calculated from the published Karplus curves (6, 18) is between  $-2.0$  and  $-3.0$  Hz, which is in good agreement with the presently measured value.

In conclusion this Communication describes a heteronuclear 3D NMR experiment for measuring small heteronuclear couplings in  ${}^{15}\text{N}$ -labeled proteins. In this experiment the observed cross peaks are generated by a  ${}^1\text{H}$  NOESY pulse sequence. Compared to a corresponding 2D NMR experiment with a  ${}^{15}\text{N}$ -labeled protein (11), a significantly improved spectral resolution was achieved. This enabled an analysis of cross peaks between amide protons and  $\alpha$  protons (Figs. 2A-2C), which are only poorly resolved in the two-dimensional experiment (11). The uncertainties of  $\pm 0.7$  Hz in the values measured for the geminal and vicinal coupling constants were estimated by comparing  $J$  values derived from different cross sections through the same cross peaks. Of course, fundamentally it is the digital resolution of 1.5 Hz/point along  $\omega_2$  that limits the accuracy of the heteronuclear coupling constants measured from these plots, so that it is quite conceivable that the accuracy of such measurements will be further improved in the future. However, as was previously suggested (11), even with the presently used digital resolution the heteronuclear  ${}^{15}\text{N}-{}^1\text{H}$  couplings have considerable potential interest as complementary conformational constraints in studies of polypeptide conformations.

#### ACKNOWLEDGMENTS

We thank Dr. C. Griesinger and Dr. R. R. Ernst for a software routine which enables processing 3D NMR data on a Bruker Aspect 1000 computer, and Mr. R. Marani for the careful processing of the typescript. Financial support by the Schweizerischer Nationalfonds (Project 31-25174.88) is gratefully acknowledged.

#### REFERENCES

1. K. WÜTHRICH, G. WIDER, G. WAGNER, AND W. BRAUN, *J. Mol. Biol.* **155**, 311 (1982).
2. K. WÜTHRICH, "NMR of Proteins and Nucleic Acids," Wiley, New York, 1986.

3. C. GRIESINGER, O. W. SØRENSEN, AND R. R. ERNST, *J. Magn. Reson.* **73**, 574 (1987).
4. S. W. FESIK AND E. R. P. ZUIDERWEG, *J. Magn. Reson.* **78**, 588 (1988).
5. D. MARION, L. E. KAY, S. W. SPARKS, D. A. TORCHIA, AND A. BAX, *J. Am. Chem. Soc.* **111**, 1515 (1989).
6. V. F. BYSTROV, *Prog. NMR Spectrosc.* **10**, 41 (1976).
7. A. PARDI, M. BILLETER, AND K. WÜTHRICH, *J. Mol. Biol.* **180**, 741 (1984).
8. P. GÜNTERT, W. BRAUN, M. BILLETER, AND K. WÜTHRICH, *J. Am. Chem. Soc.*, in press (1989).
9. J. FEENEY, P. E. HANSEN, AND G. C. K. ROBERTS, *J. Chem. Soc. Chem. Commun.*, 465 (1974).
10. D. NEUHAUS, G. WAGNER, M. VAŠÁK, J. H. R. KÄGI, AND K. WÜTHRICH, *Eur. J. Biochem.* **143**, 659 (1984).
11. G. T. MONTELIONE, M. E. WINKLER, P. RAUENBÜHLER, AND G. WAGNER, *J. Magn. Reson.* **82**, 198 (1989).
12. G. OTTING AND K. WÜTHRICH, *J. Magn. Reson.* **76**, 569 (1988).
13. D. MARION AND K. WÜTHRICH, *Biochem. Biophys. Res. Commun.* **113**, 967 (1983).
14. J. GOUGH AND N. MURRAY, *J. Mol. Biol.* **166**, 1 (1983).
15. J. ANDERSON, M. PTASHNE, AND S. C. HARRISON, *Proc. Natl. Acad. Sci. USA* **81**, 1307 (1984).
16. D. NERI, T. SZYPERSKI, G. OTTING, H. SENN, AND K. WÜTHRICH, *Biochemistry*, submitted.
17. A. MONDRAGON, S. SUBBIAH, S. C. ALMO, M. DROTTAR, AND S. C. HARRISON, *J. Mol. Biol.* **205**, 189 (1989).
18. A. DEMARCO, M. LLÍNAS, AND K. WÜTHRICH, *Biopolymers* **17**, 2727 (1978).